Dissociation Pathways of Peroxyacetyl Nitrate (PAN)

Charles E. Miller,* Julia I. Lynton, and Derek M. Keevil

Department of Chemistry, Haverford College, Haverford, Pennsylvania 19041

Joseph S. Francisco

Department of Chemistry, Purdue University, West Lafayette, Indiana 47907

Received: July 29, 1999; In Final Form: October 12, 1999

The principal unimolecular dissociation pathways for PAN (peroxyacetyl nitrate, $CH_3C(O)OONO_2$) have been studied using a variety of theoretical methods. Reaction enthalpies calculated with the complete basis set (CBS) method were evaluated against a set of atmospheric free radical reactions for which the experimental thermochemistry is well defined. The validation procedure, which included two decomposition channels for $HOONO_2$, demonstrated that the CBS-Q method reproduced the experimental ΔH_{rxn}^{298K} values with a rms error of 5.7 kJ mol^{-1}. We report new ΔH_f^{298K} values for PAN, $CH_3C(O)O_2$, and $CH_3C(O)O$ of −240.1, −154.4 and −192.5 kJ mol^{-1}, respectively. Accurate structural calculations for PAN, $HOONO_2$, $CH_3C(O)O_2$, and $CH_3C(O)O$ augment the thermochemical calculations and show that the B3LYP density functional method describes the chemical bonding in the $-OONO_2$ linkage quite well. The implications of this study for the atmospheric decomposition of PAN are discussed.

Introduction

Peroxy nitrates, $ROONO_2$, are important organic contributors to photochemical smog, acting as temporary reservoirs of both RO_2 and NO_x. The most well-known member of this class, PAN (peroxyacetyl nitrate, $CH_3C(O)OONO_2$), was first identified by Stephens et al. during smog episodes in the Los Angeles basin in the 1950s.[1] Subsequent studies have shown that not only is PAN found in NO_x-rich urban environments, but that it also constitutes one of the most abundant reactive nitrogen-containing species in the clean troposphere.[2,3] PAN forms in urban areas where the photochemistry of nonmethane hydrocarbons coincides with high NO_x concentrations and exists in a rapid equilibrium with its radical precursors

$$CH_3C(O)OONO_2 + M \rightarrow CH_3C(O)OO + NO_2 + M \quad (R1)$$

Convective action transports PAN into the upper troposphere where it may travel hundreds of kilometers before descending in a remote location. Since PAN is a temporary NO_x reservoir, the net result of this long-range transport is to redistribute NO_x from polluted urban environments into pristine environments where normal NO_x concentrations are otherwise negligible.

The weak O−O and O−N bonds in PAN and other peroxy nitrates cause these molecules to undergo facile thermal decomposition at ambient pressure and temperatures, ca. 760 Torr and 300 K.[4−9] Thermal decomposition is, in fact, the principal loss mechanism for PAN at ground level. However, PAN thermal decomposition rates decrease dramatically under the conditions of the upper troposphere, ca. 100 Torr and 220 K, and photolysis becomes the major loss process above approximately 8 km.[10] It is clear that accurate modeling of the long-range transport of PAN requires reliable thermochemical values for PAN and its radical constituents for all relevant atmospheric conditions. The large uncertainties in the recommended values of these key parameters[11,12] motivated the present study.

Numerous experimental studies[4−6,13−15] have shown that the thermal decomposition of PAN occurs only via the NO_2 producing channel (nitrate O−N bond cleavage)

$$CH_3C(O)OONO_2 \rightarrow CH_3C(O)OO + NO_2 \quad (R1a)$$

with no contribution from the NO_3 producing channel (peroxy O−O bond cleavage)

$$CH_3C(O)OONO_2 \rightarrow CH_3C(O)O + NO_3 \quad (R1b)$$

even though the channels are predicted to be nearly isoenergetic.[11,12] It has been argued that the thermal decomposition via R1a is favored over R1b because R1a dissociation proceeds without a barrier;[4] however, the thermochemistry of PAN, $CH_3C(O)O_2$, and $CH_3C(O)O$ is poorly defined, so the actual reaction enthalpies have uncertainties of at least 20 kJ mol^{-1}. Additionally, the 248 nm photodissociation experiments performed by Mazely, Friedl, and Sander[16,17] demonstrated significant quantum yields for both channels, $\phi(R1a) = 0.89 \pm 0.09$ and $\phi(R1b) = 0.30 \pm 0.10$ so that, if there is a barrier to dissociation via R1b, it is surmountable at fairly low energies.

Despite the interesting thermochemical and structural questions posed by the bonding in PAN, there have been few theoretical treatments of this molecule. Domalski[18] estimated ΔH_f^{298K} of PAN at -238 ± 8.4 kJ mol^{-1} using bond additivity methods. Bridier et al. used semiempirical calculations in combination with their experimental value of $\Delta H_{rxn}^{298K} = 118.8 \pm 4.0$ kJ mol^{-1} for R1a to estimate $\Delta H_f^{298K} = -258 \pm 22$ kJ mol^{-1} for PAN.[19] Jursic[20] calculated 104 kJ mol^{-1} for R1a using density functional theory. There has been somewhat more effort placed into calculations on PNA (peroxy nitric acid, $HOONO_2$), the prototypical peroxy nitrate. Saxon and Liu explored the

* Corresponding author. E-mail: cmiller@haverford.edu.

10.1021/jp992667h CCC: $18.00
Published on Web 11/25/1999

TABLE 1: Optimized $HOONO_2$ Structures and Energies

		B3LYP							
theory basis set	CBS-Q	6-31 G*	6-31 G(d,p)	6-31 G(2d,2p)	6-311 G(2df,2pd)	6-311++ G(2df,2pd)	6-311++ G(3df,3pd)	CCSD(T) cc-pVDZ	expt[a]
				Bond Lengths/Å					
HO_1	0.948	0.978	0.975	0.971	0.969	0.970	0.970	0.976	0.965
O_1O_2	1.358	1.404	1.405	1.398	1.398	1.398	1.396	1.418	1.464
O_2N	1.373	1.511	1.511	1.504	1.512	1.514	1.513	1.518	1.515
NO_3	1.165	1.199	1.199	1.193	1.188	1.189	1.188	1.200	1.196
NO_4	1.167	1.198	1.198	1.192	1.187	1.187	1.186	1.200	1.226
				Angles/deg					
HO_1O_2	105.0	102.7	102.8	103.0	103.1	103.4	103.4	101.6	99.4
O_1O_2N	111.4	109.1	109.0	109.1	109.3	109.8	109.6	108.1	101.2
O_2NO_3	111.5	110.2	110.2	110.1	110.0	109.9	109.9	109.9	115.8
O_2NO_4	117.7	116.5	116.5	116.5	116.3	116.5	116.5		115.2
O_3NO_4	130.7	133.3	133.3	133.3	133.6	133.6	133.6	133.5	129.0
				Dihedral Angle/deg					
HO_1O_2N	84.8	85.3	84.6	84.0	85.5	88.0	87.5	84.2	106.2
$O_1O_2NO_3$	165.9	171.0	170.8	171.5	171.3	171.7	171.9	177.9	180.0
$O_1O_2NO_4$	−16.2	−10.5	−10.6	−9.9	−9.9	−9.3	−9.2	−12.2	0.0
energy/hartrees	−355.620970	−356.007796	−356.012880	−356.033513	−356.140683	−356.153845	−356.157357	−355.196093	

[a] Reference 52.

$HOONO_2$ equilibrium structure and vertical excitation energies using SCF and Møller−Plesset perturbation theory.[21] More recently, Chen and Hamilton have reinvestigated the $HOONO_2$ structure using even more sophisticated levels of theory.[22] They also calculated the $HOO-NO_2$ bond dissociation energy with the complete basis set[23] method. Jursic used density functional theories to examine several possible structures for PNA for comparison against his PAN results.[20]

In an effort to understand the PAN thermal decomposition process and provide more accurate thermochemical data for PAN and its free radical decomposition products, we have investigated the decomposition pathways and molecular structure of PAN using a variety of theoretical methods. The theoretical enthalpies obtained in these calculations have been validated using a number of atmospheric free radical reactions for which the thermodynamics are well-known. As an additional check, we have investigated the dissociation pathways of $HOONO_2$ to ensure that our results are not subject to systematic errors when treating peroxy nitrates. The results of this study provide useful information for current atmospheric modeling efforts and will guide future investigations into the thermochemistry of C2, C3, and larger organic peroxynitrates.

Methodology

All structure optimizations and thermochemical calculations were performed using the Gaussian 98 program suite.[24] The project was initiated at Haverford College using a 400 MHz Pentium II based personal computer running Gaussian 98W.[24] However, the limited hardware resources of the personal computer prevented it from completing the larger calculations successfully. More computationally intensive calculations, including most of the structure optimizations for PAN and the organic radicals, were performed using Gaussian 98[24] on the JPL Cray J90.

Optimized structures were computed using the second-order Møller−Plesset (MP2),[25−28] Becke3-Lee−Yang−Parr (B3LYP) density functional[29] and coupled cluster with singles, doubles, and partial triples (CCSD(T))[30] levels of theory. Basis sets 6-31G through 6-311++G(3df,3pd)[31−37] and cc-PVDZ[38−43] contained in Gaussian were used without modification. Thermochemical information was calculated using the complete basis set (CBS) methods CBS-4,[44] CBS-q,[23,45] CBS-Q,[44] CBS-QB3,[46] as well as the G1[47,48] and G2[49−51] algorithms. Temperature-dependent CBS-Q reaction enthalpies were calculated in a series of rapid jobs from the stored output of the initial CBS-Q results. Reaction enthalpies were also estimated by adding the CBS-Q zero-point energies to the B3LYP/6-311++G(3df,3pd) energies obtained for all components of R1 and R2.

Results and Discussion

The goal of this project was to study the unimolecular dissociation of PAN with accurate theoretical methods in an effort to reduce the large uncertainties in the thermochemical parameters associated with this process. Preliminary calculations demonstrated that Møller−Plesset perturbation theory, configuration interaction, coupled cluster, and G2 approaches were not feasible for PAN-type molecules. Therefore, density functional and the complete basis set (CBS) methods were employed to produce reliable thermochemical predictions with reasonable computational expense. The theoretical and experimental data for $HOONO_2$, the prototypical peroxynitrate, were compared in detail to evaluate these methods. The strengths and weaknesses of the $HOONO_2$ calculations guide the interpretation of the PAN results and suggest possible trends in the theoretical estimates of thermochemical parameters for more complicated PAN-type molecules.

1. Molecular Structures. The $-OONO_2$ group in peroxy nitrates provides a rigorous challenge to ab initio calculations as well as to experiment. This is a branched-chain functional group with five consecutive electronegative atoms. The nitrogen atom bonds nonequivalently with the three oxygen atoms to which it is connected and the orientation of the peroxy bond influences the bonding characteristics of the two oxygen atoms in the $-NO_2$ group. Finally, both the $ROO-NO_2$ and $RO-ONO_2$ bonds are relatively weak, with dissociation energies in the 100−200 kJ mol^{-1} range.[11,12]

$HOONO_2$ structural calculations provide a stringent test of the performance of the theoretical methods used in this study since an approximate experimental structure has been inferred from the $HOONO_2$ microwave spectrum.[52] The optimized $HOONO_2$ structures are collected in Table 1. The B3LYP calculations converge to a single structure as the basis set increases from 6-31G(d) to 6-311++G(3df,3pd). The characteristic structure consists of a nearly planar heavy atom

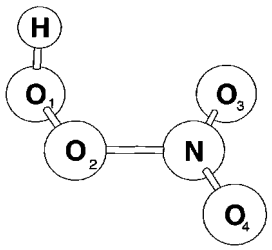

Figure 1. A depiction of the optimized $HOONO_2$ structure. The heavy atom frame is nearly planar with the H atom oriented perpendicular to the plane.

TABLE 2: $HOONO_2$ Rotational Constants and Dipole Moments

	B3LYP/6-311G (2df,2pd)	B3LYP/6-311++G (3df,3pd)	CCSD(T) cc-pVDZ	experimental[a]
		Rotational Constant/MHz		
A	12061	12068	11788	11994
B	4642	4628	4613	4665
C	3392	3384	3358	3397
		Dipole Moment/debye		
μ_A	1.304	1.383	1.662	1.185
μ_B	0.532	0.517	0.553	0.940
μ_C	1.442	1.446	1.607	1.288

[a] Reference 52.

framework with the hydrogen atom rotated almost perpendicular to this plane (see Figure 1). This agrees with the microwave spectrum in which tunneling splittings in the ground vibrational state transitions indicate a planar $-OONO_2$ frame with the H atom undergoing rapid torsional inversion between two equivalent conformers. The slight discrepancy between the HOON and $OONO_2$ dihedral angles in the B3LYP and experimental structures is not unexpected since the potentials along these large amplitude motion coordinates should be relatively flat, making it difficult to identify the exact equilibrium positions. We note that the experimental structure was derived from the geometries of HNO_3 and HOOH;[52] a substitution structure has not been determined. Additionally, the actual equilibrium configuration of the heavy atom frame may be nonplanar even though it appears to be planar in the vibrational ground state.

The reliability of the B3LYP/6-311++G(3df,3pd) structure is further corroborated by the optimized CCSD(T)/cc-pVDZ structure (Table 1). The CCSD(T) result comes closer to reproducing the planar peroxy nitrate group and exhibits a slight lengthening of the peroxy O−O bond, but otherwise there is little to distinguish it from the best B3LYP structure. It is interesting to observe that both the B3LYP and CCSD(T) structures predict that the HOON dihedral angle is slightly less than 90° while the experimental estimate was slightly larger than 90°.[52]

The theoretical and experimental rotational constants and dipole moments presented in Table 2 show good agreement. The theoretical structures reproduce the *B* and *C* rotational constants very well; the small differences are probably due to slight inaccuracies in the nonplanar deformation of the heavy atom frame. The experimental and theoretical *A* rotational constants exhibit larger differences. Since the value of *A* is dominated by contributions from the HOON dihedral angle and the HO bond length, the differences suggest that the theoretical values for these two parameters require further refinement. Surprisingly, the B3LYP/6-311G(2df,2pd) level of theory reproduces the experimental values better than the B3LYP/6-311++G(3df,3pd) or CCSD(T)/cc-pVDZ calculations. This is most likely a fortuitous result, but it appears that the B3LYP density functional coupled with a large, high quality basis set reproduces the salient structural features of the peroxy nitrate group and should be reliable for predicting the PAN structure.

The optimized PAN structures are collected in Table 3. The most interesting aspect of the PAN geometry is that the acetyl group is oriented perpendicularly to the peroxy nitrate group. In fact, the $-OONO_2$ group in PAN is calculated to be more planar than in $HOONO_2$. The molecular structure is shown in Figure 2. There has been no experimental determination of the PAN structure, but the results presented here indicate that aside from the orientation of the acetyl and peroxy nitrate groups there are no unusual geometric parameters. Jursic reported a B3LYP/6-31+G(d) structure for PAN that is consistent with the results in Table 3 at low levels of theory.[20]

The only previous report of any structural information for the $CH_3C(O)O_2$ radical is from the LCGTO-LSD calculations of Sicilia et al.;[53] therefore, we provide the B3LYP structural optimizations for this species in Table 4. There have been several theoretical calculations of the $CH_3C(O)O$ structure due to its high symmetry, [54,55] and these are compared with the results of the present study in Table 5. The rotational constants and dipole moments for PAN, $CH_3C(O)O_2$, and $CH_3C(O)O$ are given in Table 6. All three molecules are calculated to have substantial dipole moments and should present strong rotational spectra.

2. $HOONO_2$ Thermochemistry. The calculation of thermochemical parameters for PAN and its dissociation pathways presented an imposing challenge: In addition to obtaining a reliable ΔH_f^{298} for PAN, this also required obtaining accurate ΔH_f^{298} values for all of the radical decomposition products. Since the most accurate thermochemical calculation methods obtain accurate molecular energies by calculating higher order corrections with post-Hartree−Fock methods, it was unclear how the G2 and CBS methods would perform for PAN or its radical components. In contrast, the thermodynamics associated with $HOONO_2$ and its radical components were relatively well defined. Therefore, we investigated the $HOONO_2$ decomposition in detail and used the results to guide our interpretation of the PAN dissociation thermochemistry.

The recommended ΔH_{rxn}^{298} values for $HOONO_2$ decomposition via the channels

$$HOONO_2 \rightarrow HO_2 + NO_2 \qquad \text{(R2a)}$$

$$\rightarrow OH + NO_3 \qquad \text{(R2b)}$$

were calculated from the tabulated heats of formation and are presented in Table 7. All experimental studies to date indicate that R2a is the sole pathway accessed in thermal decomposition of $HOONO_2$. Zabel determined $\Delta H_{rxn}^{298} = 99.6 \pm 3.1$ kJ mol^{-1} for R2a based on the temperature dependence of the thermal decomposition rate and the $HO_2 + NO_2$ recombination rate.[4] The JPL 97-4 ΔH_{rxn}^{298} value of 97.1 ± 8.6 kJ mol^{-1} agrees with the experimental value and can be modified to 99.2 ± 9.0 kJ mol^{-1} by using the $\Delta H_f^{298}(HO_2) = 13.8 \pm 3.3$ kJ mol^{-1} determined by Litorja and Ruscic[56] instead of 11.7 ± 2.1 kJ mol^{-1}. In fact, calculating the $HOONO_2$ heat of formation from the Zabel ΔH_{rxn}^{298} for R2a, the Litorja and Ruscic $\Delta H_f^{298}(HO_2)$ and $\Delta H_f^{298}(NO_2)$ yields $\Delta H_f^{298}(HOONO_2) = -52.7 \pm 4.5$ kJ mol^{-1}. This is in excellent agreement with the value currently recommended by DeMore et al., -52.3 ± 8.4 kJ mol^{-1}, but with about one-half the uncertainty. Atkinson et al.[12] recommend $\Delta H_f^{298}(HOONO_2) = -57$ kJ mol^{-1} and this accounts for the discrepancy between the JPL and IUPAC reaction enthalpies presented in Table 7.

TABLE 3: Theoretical Structures for PAN

		B3LYP/			
theory basis set	CBS-Q	6-31G*	6-311 G(d,p)	6-311 G(2d,2p)	6-311 G(2df,2p)	6-311++ G(3df,3pd)
			Bond Lengths/Å			
C−H1	1.082	1.091	1.088	1.085	1.085	1.085
C−H2	1.086	1.095	1.093	1.090	1.090	1.090
C−H3	1.086	1.094	1.090	1.089	1.089	1.089
C1−C2	1.500	1.506	1.502	1.502	1.501	1.500
C═O1	1.167	1.195	1.187	1.187	1.186	1.186
C−O	1.378	1.406	1.408	1.405	1.402	1.403
O2−O3	1.352	1.410	1.403	1.404	1.401	1.398
O3−N	1.378	1.508	1.524	1.512	1.512	1.512
N−O4	1.163	1.197	1.187	1.189	1.186	1.185
N−O5	1.165	1.197	1.188	1.188	1.186	1.185
			Angles/deg			
C1−C2═O1	129.1	128.9	129.0	128.8	128.9	128.9
C1−C2−O2	108.3	107.5	107.6	107.7	107.6	107.8
O1═C2−O2	122.6	123.5	123.4	123.5	123.5	123.3
C2−C1−H1	108.7	108.6	108.6	108.6	108.7	108.7
C2−C1−H2	109.5	109.4	108.8	109.4	109.4	109.5
C2−C1−H3	110.0	111.0	111.3	110.7	110.8	110.7
H1−C1−H2	110.1	109.5	109.2	109.8	109.7	109.8
H1−C1−H3	110.3	110.4	110.7	110.5	110.5	110.4
H2−C1−H3	108.2	107.9	108.1	107.9	107.8	107.8
C2−O2−O3	112.4	111.3	111.9	111.4	111.7	111.9
O2−O3−N	111.4	109.2	109.5	109.4	109.5	109.6
O3−N−O4	110.8	109.4	109.4	109.3	109.3	109.4
O3−N−O5	118.0	117.0	116.6	116.8	116.7	116.6
O4−N−O5	131.1	133.6	134.1	133.8	134.0	133.9
			Dihedral Angles/deg			
H1−C1−C2═O1	1.9	11.4	19.8	8.0	9.4	7.0
H2−C1−C2═O1	−118.5	−108.0	−99.0	−111.8	−110.4	−112.9
H3−C1−C2═O1	122.7	133.0	142.0	129.5	130.9	128.4
H1−C1−C2−O2	−178.5	−169.7	−161.6	−172.8	−171.6	−173.9
H2−C1−C2−O2	61.2	70.8	79.7	67.4	68.7	66.2
H3−C1−C2−O2	−57.6	−48.2	−39.4	−51.4	−50.0	−52.5
C1−C2−O2−O3	176.5	177.8	178.1	177.2	177.4	177.0
O1 = C2−O2−O3	−3.8	−3.3	−3.1	−3.6	−3.5	−3.8
C2−O2−O3−N	88.5	85.1	85.4	85.9	85.7	85.6
O2−O3−N−O4	175.6	177.4	177.2	177.3	177.4	177.8
O2−O3−N−O5	−4.3	−2.3	−2.5	−2.4	−2.2	−1.8
energy/hartrees	−507.351997	−508.671708	−508.817626	−508.835209	−508.850462	−508.870163

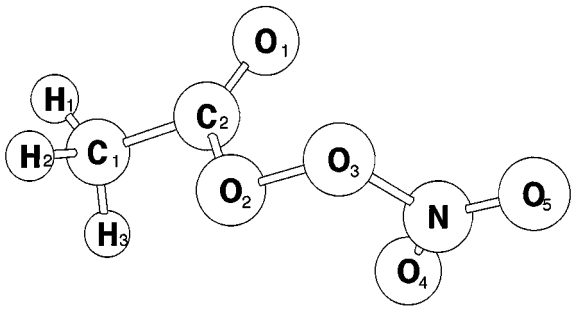

Figure 2. An illustration of the optimized PAN structure demonstrating the perpendicular orientation of the acetyl and peroxy nitrate groups.

There has been no experimental determination of ΔH_{rxn}^{298}(R2b), but this value may be calculated from the tabulated heats of formation. We note that the enthalpy difference between R2a and R2b may be determined independently of ΔH_f^{298}(HO-ONO_2). Values for ΔH_{rxn}^{298}(R2b) range from 165 to 170 kJ mol^{-1} depending on the ΔH_f^{298}($HOONO_2$) assumed, but there is good agreement that the $\Delta(\Delta H_{rxn}^{298})$ is 66.5 ± 1.0 kJ mol^{-1}. This large energy difference is consistent with the observed products of $HOONO_2$ thermal dissociation.

Theoretical ΔH_{rxn}^{298} for R2a and R2b were determined by calculating the ΔH_f^{298} values for $HOONO_2$, HO_2, NO_2, OH, and NO_3 using each of the methods listed in Table 7. All of the theoretical methods predict that ΔH_{rxn}^{298}(R2a) is substantially lower than ΔH_f^{298}(R2b), but there is a noticeable variation in the quantitative agreement between the different predictions and the experimental thermochemistry. The G1 and G2 methods overestimate ΔH_{rxn}^{298} for each of the dissociation channels and the net separation between channels by approximately 10 kJ mol^{-1}. The CBS-4 and CBS-q calculations predict ΔH_{rxn}^{298}(R2a) more reasonably, but severely underestimate the enthalpy difference between R2a and R2b. The CBS-Q and CBS-QB3 calculations provide thermochemical predictions that reproduce Zabel's experimental ΔH_{rxn}^{298}(R2a) to within experimental uncertainty.

The ability of the CBS-Q and CBS-QB3 methods to calculate accurate $HOONO_2$ bond energies is further emphasized by the good agreement between the experimental and theoretical values for ΔH_{rxn}^{298}(R2b). The best experimental estimate of ΔH_{rxn}^{298}(R2b) appears to be 165 ± 6 kJ mol^{-1}. The CBS-Q value of 173.6 kJ mol^{-1} lies just above the experimental uncertainty limit, although it falls within the uncertainty limits of the JPL 97-4 recommendation. The CBS-QB3 calculation produces ΔH_{rxn}^{298}(R2b) = 163.8 kJ mol^{-1} which is somewhat low, but well within the experimental uncertainty. Note that the CBS-Q and CBS-QB3 reproduce both the absolute values of

TABLE 4: Optimized Structures for $CH_3C(O)O_2$

theory / basis set	CBS-Q	B3LYP 6-31G*	B3LYP 6-311 G(d,p)	B3LYP 6-311 G (2d,2p)	B3LYP 6-311 G (2df,2p)	B3LYP 6-311++ G (3df,3pd)	LCGTO LSD[a]
			Bond Lengths/Å				
H_1-C_1	1.082	1.090	1.088	1.085	1.085	1.090	1.103
H_2-C_1	1.086	1.095	1.092	1.090	1.090	1.090	1.098
H_3-C_1	1.086	1.095	1.092	1.090	1.090	1.090	1.098
C_1-C_2	1.502	1.501	1.498	1.496	1.496	1.495	1.475
$C_2=O_1$	1.167	1.190	1.181	1.180	1.180	1.179	1.189
C_2-O_2	1.380	1.447	1.452	1.450	1.446	1.452	1.456
O_2-O_3	1.305	1.328	1.322	1.322	1.319	1.316	1.310
			Angles/deg				
$H_1-C_1-H_2$	110.2	110.0	110.2	110.2	110.2	110.2	
$H_1-C_1-H_3$	110.2	110.0	110.2	110.2	110.2	110.2	
$H_1-C_1-C_2$	109.0	109.2	109.2	109.2	109.2	109.3	109.0
$H_2-C_1-H_3$	107.9	107.4	107.4	107.4	107.4	107.4	
$H_2-C_1-C_2$	109.8	110.0	109.9	109.8	109.9	109.8	109.7
$H_3-C_1-C_2$	109.8	110.0	109.9	109.8	109.9	109.8	109.7
$C_1-C_2=O_1$	128.3	129.9	130.3	130.0	130.2	130.3	131.2
$C_1-C_2-O_2$	108.6	107.6	107.6	107.7	107.6	107.6	107.5
$O_1=C_2-O_2$	123.1	122.5	122.2	122.3	122.4	122.2	
$C_2-O_2-O_3$	114.2	113.1	113.6	113.1	113.4	113.5	113.0
			Dihedral Angles/deg				
$H_1-C_1-C_2=O$	0.0	0.0	0.0	0.0	0.0	0.0	
$H_1-C_1-C_2-O_2$	−180.0	−180.0	−180.0	−180.0	−180.0	−180.0	
$H_2-C_1-C_2=O_1$	−120.8	−120.9	−121.0	−121.0	−121.0	−121.0	
$H_2-C_1-C_2-O_2$	59.2	59.1	59.0	59.0	59.0	59.0	
$H_3-C_1-C_2=O_1$	120.8	120.9	121.0	121.0	121.0	121.1	
$H_3-C_1-C_2-O_2$	−59.2	−59.1	−58.9	−59.0	−59.0	−58.9	
$C_1-C_2-O_2-O_3$	180.0	−180.0	180.0	−180.0	−180.0	−180.0	
$O_1=C_2-O_2-O_3$	0.0	0.0	0.0	0.0	0.0	0.0	
energy/hartrees	−303.151450	−303.556092	−303.643931	−303.654395	−303.662179	−303.674406	

[a] Reference 53.

TABLE 5: $CH_3C(O)O$ Optimized Geometries

theory / basis set	CBS-Q	B3LYP/ 6-311++G (3df,3pd)	B3PW91 6-311++G (3df,3pd)[a]	MP2 6-31G(d)[b]	LCGTO LSD[c]
		Bond Lengths/Å			
H_1-C	1.094	1.088	1.092	1.092	1.102
H_2-C	1.096	1.090	1.089	1.092	1.103
H_3-C	1.096	1.090	1.089	1.092	1.103
$C-C$	1.515	1.489	1.485	1.491	1.471
$C-O_1$	1.210	1.254	1.252	1.265	1.260
$C-O_2$	1.339	1.256	1.252	1.265	1.260
		Angles/deg			
H_1-C-C	107.7	110.3	110.1	109.6	110.3
H_2-C-C	110.5	109.3	108.8	109.6	108.7
H_3-C-C	110.5	109.3	108.8	109.6	108.7
$C-C-O_1$	127.6	124.4	124.4		124.2
$C-C-O_2$	110.8	124.0	124.4		124.2
O_1-C-O_2	121.6	111.5		110.2	
H_1-C-H_2	109.9	109.9			
H_2-C-H_3	108.3	108.0			
H_1-C-H_3	109.9	109.9			
		Dihedral Angles/deg			
$H_1-C-C-O_1$	0.0	0.0			
$H_2-C-C-O_1$	−120.1	−121.0			
$H_3-C-C-O_1$	120.1	121.0			
$H_1-C-C-O_2$	180.0	180.0			
$H_2-C-C-O_2$	59.9	59.0			
$H_3-C-C-O_2$	−59.9	−59.0			
energy/hartrees	−228.079108	−228.501617			−228.748962

[a] Reference 55. [b] Reference 54. [c] Reference 53.

ΔH^{298}_{rxn}(R2a) and ΔH^{298}_{rxn}(R2b) as well as $\Delta(\Delta H^{298}_{rxn})$ extremely well. The excellent performance of the CBS-Q and CBS-QB3 methods in evaluating the thermochemistry associated with $HO-ONO_2$ dissociation suggests that these methods should be well suited for evaluating the thermochemistry of PAN dissociation.

3. PAN Thermochemistry. PAN dissociates via cleavage of the weak $ROO-NO_2$ or $RO-ONO_2$ bonds

$$CH_3C(O)OONO_2 \rightarrow CH_3C(O)OO + NO_2 \quad \text{(R1a)}$$

$$\rightarrow CH_3C(O)O + NO_3 \quad \text{(R1b)}$$

All experimental investigations of PAN thermal dissociation reported to date agree that the decomposition proceeds exclusively via R1a for temperatures less than 350 K. However, inspection of the parameters in Table 8 reveals that the recommended thermochemical values place ΔH^{298}_{rxn}(R1a) only 5 kJ mol^{-1} below ΔH^{298}_{rxn}(R1b) and that the uncertainty of these values is so large that even the energetic ordering of the dissociation channels should be questioned. The small differences in ΔH^{298}_{rxn} predicted from the recommended thermochemistry clearly contradict the experimental evidence since there should have been some observation of NO_3 or $CH_3C(O)O$ in the PAN thermal dissociation measurements if

TABLE 6: Rotational Constants and Dipole Moments for PAN, $CH_3C(O)O_2$, and $CH_3C(O)O$[a]

	PAN	$CH_3C(O)O_2$	$CH_3C(O)O$
	Rotational Constant/MHz		
A	5079	10474	13441
B	1290	4419	9271
C	1283	3168	5680
	Dipole Moment/debye		
μ_X	−2.869	−3.094	−3.352
μ_Y	1.660	−1.864	−0.078
μ_Z	0.815	0.000	0.000
μ_{TOT}	3.413	3.612	3.353

[a] All values calculated from the optimized B3LYP/6-311++G(3df,3pd) structures.

TABLE 7: Calculated Reaction Enthalpies (kJ mol^{-1}) for $HOONO_2 \rightarrow HO_2 + NO_2$ (R2a) $\rightarrow OH + NO_3$ (R2b)

theory	R2a ΔH^{298}_{rxn}	R2b ΔH^{298}_{rxn}	R2b − R2a $\Delta(\Delta H^{298}_{rxn})$
G1	113.4	190.9	77.5
G2	109.0	187.2	78.2
CBS-4	106.8	154.9	48.1
CBS-q	96.7	142.6	45.9
CBS-Q	100.1	173.6	73.5
CBS-QB3	102.8	163.8	61.0
CBS-q[a]	92.0	133.8	41.8
B3LYP[b]	88.4		
IUPAC VI[c]	104.8	170.0	65.2
JPL 97-4[d]	97.1 ± 8.6	164.8 ± 9.4	67.7 ± 4.7
JPL 97-4 adj	99.2 ± 9.0	164.8 ± 9.4	65.6 ± 5.3
exptl[e]	99.6 ± 3.1	(167.3 ± 5.6)[f]	(67.7 ± 4.7)
		(165.2 ± 6.1)	(65.6 ± 5.3)

[a] Reference 22. [b] Reference 20. B3LYP/6-311+G(3df,3pd)//B3LYP/6-31+G(d) calculation. [c] Reference 11. [d] Reference 12. [e] Reference 4. [f] Estimated from refs 4 and 11.

TABLE 8: Calculated Reaction Enthalpies (kJ mol^{-1}) for $CH_3C(O)OONO_2 \rightarrow CH_3C(O)O_2$ (R1a) $\rightarrow CH_3C(O)O + NO_3$ (R1b)

theory	R1a $\Delta H^{\circ,298K}_{rxn}$	R1b $\Delta H^{\circ,298K}_{rxn}$	R1b−R1a $\Delta(\Delta H^{\circ,298K}_{rxn})$
CBS-4	140.5	154.7	14.2
CBS-q	133.8	139.1	5.3
CBS-Q	128.4	157.4	29.0
B3LYP[a]	106		
IUPAC[b]	119.2	124.2	5.0
JPL97−4[c]	120.9 ± 29.6	125.5 ± 23.5	4.6 ± 23.5
exptl[d]	118.8 ± 4.0		
exptl[e]	120.6 ± 5.8		

[a] Reference 20. B3LYP/6-311+G(3df,3pd)//B3LYP/6-31+G(d) calculation. [b] Reference 12. No uncertainties listed. [c] Reference 11. [d] Reference 19. [e] Reference 4.

ΔH^{298}_{rxn}(R1b) were only 5 kJ mol^{-1} more endothermic than ΔH^{298}_{rxn}(R1a).

The only reliable experimental information for PAN concerns ΔH^{298}_{rxn}(R1a) which has been reported as 118.8 ± 4.0 kJ mol^{-1} by Bridier et al.[19] and 120.6 ± 5.8 kJ mol^{-1} by Zabel.[4] These reaction enthalpies were determined from the temperature dependence of the thermal dissociation rate and the recombination rate. All other thermochemical parameters associated with the PAN system have been deduced from ΔH^{298}_{rxn}(R1a) and some estimate of ΔH^{298}_f for PAN and/or $CH_3C(O)O_2$. The large uncertainties in these estimates account for the large uncertainty limits for the enthalpies calculated from the recommended values.[11,12]

Enthalpies for a series of HO_x and NO_x atmospheric free radical reactions, including two $HOONO_2$ dissociation reactions, were calculated using the CBS-Q method to verify that this method accurately reproduces experimental thermochemistry for peroxy nitrates and their decomposition products. The results of these calculations are presented in Table 9 as absolute differences from the ΔH^{298}_{rxn} values calculated from the DeMore et al. recommendations.[11] The rms deviation of the CBS-Q ΔH^{298}_{rxn} values was 5.68 kJ mol^{-1} which provides an approximate figure of merit for comparison with other reaction sets and is consistent with the findings of other groups.[57−61]

TABLE 9: Comparison of Recommended and Theoretical Reaction Enthalpies (kJ mol^{-1}) for Relevant Atmospheric Free Radical Reactions

reaction	JPL 97-4	Δ[a]
$H + O_2 \rightarrow HO_2$	−206.2	−2.9
$OH + O \rightarrow HO_2$	−276.4	−3.2
$NO_2 \rightarrow NO + O$	306.4	−6.9
$NO_3 \rightarrow NO_2 + O$	208.7	7.5
$NO_3 \rightarrow NO + O_2$	16.6	0.9
$HO_2 + NO \rightarrow OH + NO_2$	−30.0	10.1
$OH + NO_2 \rightarrow HONO_2$	−207.1	−1.9
$H + NO_2 \rightarrow OH + NO$	−121.9	−6.2
$HO_2 + NO_2 \rightarrow OH + NO_3$	67.8	−4.3
$HOONO_2 \rightarrow HO_2 + NO_2$	97.1	−3.0
$HOONO_2 \rightarrow OH + NO_3$	164.8	−7.3
		$\sigma = 5.68$

[a] $\Delta = \Delta H^{298K}_f$ (JPL 97−4) − ΔH^{298K}_f (CBS-Q).

TABLE 10: PAN and RO_x Reaction Enthalpies (kJ mol^{-1})

reaction	JPL	Δ[a]	Δ(adj)
$CH_3 + CO \rightarrow CH_3CO$	−45.9	−1.2	−1.1
$CH_3CO + O_2 \rightarrow CH_3C(O)O_2$	−161.5	−17.1	0.0
$CH_3CO + O \rightarrow CH3C(O)O$	−446.7	−13.6	1.4
$CH_3 + CO_2 \rightarrow CH_3C(O)O$	39.6	−20.1	−5.1
$CH_3COOH + OH \rightarrow CH_3C(O)O + H_2O$	−56.1	−16.2	−1.2
$CH_3COOH + HO_2 \rightarrow CH_3C(O)O + HOOH$	76.6	−13.5	−0.6
$CH_3C(O)O_2 + NO \rightarrow CH_3C(O)O + NO_2$	−93.2	10.1	8.0
$CH_3C(O)O_2 + OH \rightarrow CH_3C(O)O + HO_2$	−63.2	0.0	−0.1
$CH_3C(O)O_2 + O \rightarrow CH_3C(O)O + O_2$	−285.2	3.5	1.4
$PAN + HO_2 \rightarrow CH_3C(O)O_2 + HOONO_2$	23.8	−4.5	−8.7
$CH_3C(O)O + NO \rightarrow CH_3CO + NO_2$	140.3	20.5	5.6
$CH_3C(O)O + OH \rightarrow CH_3CO + HO_2$	170.3	10.4	−2.5
$CH_3C(O)O + O \rightarrow CH_3CO + O_2$	−51.8	13.9	−1.0
$PAN + OH \rightarrow CH_3C(O)O + HOONO_2$	−39.3	−4.5	−8.8
		$\sigma = 12.80$	$\sigma = 4.62$
$PAN \rightarrow CH_3C(O)O_2 + NO_2$	120.9	−7.5	−9.6
$PAN \rightarrow CH_3C(O)O + NO_3$	125.5	−11.9	−16.2
$CH3C(O)O_2 + NO_2 \rightarrow CH_3C(O)O + NO_3$	4.6	−4.3	−6.5

[a] $\Delta = \Delta H^{298K}_f$ (JPL 97−4) − ΔH^{298K}_f (CBS-Q).

The CBS-Q ΔH^{298}_{rxn} values for R1a, R1b, and the $\Delta(\Delta H^{298}_{rxn})$ reaction

$$CH_3C(O)O_2 + NO_2 \rightarrow CH_3C(O)O + NO_3 \qquad (R3)$$

presented in Table 10 differ from the recommended values by as much as 11.9 kJ mol^{-1}. This is beyond the limits of the expected error limits of the CBS-Q calculations established in Table 9 and suggests systematic errors in the recommended thermochemistry. This conclusion is verified in Table 10 where we demonstrate that the rms deviation between the JPL and CBS-Q reaction enthalpies is 12.80 kJ mol^{-1} for a series of PAN and RO_x reactions. The second column of Table 10 provides evidence of our initial assumption that the PAN thermochemistry currently recommended for atmospheric modeling contains gross inaccuracies. The remaining problem is to develop a PAN thermochemistry that is theoretically consistent as well as consistent with all existing experimental data.

Accurate PAN thermochemistry necessarily hinges on the experimental determination

$$CH_3C(O)OONO_2 \rightarrow CH_3C(O)O_2 + NO_2 \qquad \Delta H_{rxn}^{298} = 118.8 \pm 4.0 \text{ kJ mol}^{-1} \quad \text{(R1a)}$$

and heats of formation for two of the three molecular components; the remaining ΔH_f^{298} value could then be determined from the thermochemical cycle. The simple formation chemistry of the acetyl peroxy radical

$$CH_3CO + O_2 \rightarrow CH_3C(O)O_2 \qquad \text{(R4)}$$

suggests that $\Delta H_f^{298}(CH_3C(O)O_2)$ may be readily determined if $\Delta H_f^{298}(CH_3CO)$ is known. Fortuitously, the heat of formation for the acetyl radical has been accurately determined by recent experimental[62] and theoretical[63] work: $\Delta H_f^{298}(CH_3CO) = -10.0 \pm 1.2$ kJ mol^{-1}. A comparison of the experimental and CBS-Q ΔH_{rxn}^{298} for

$$CH_3 + CO \rightarrow CH_3CO \qquad \text{(R5)}$$

demonstrates that the CBS-Q value is in near perfect agreement with the experimental value (Table 10). We thus assume that CBS-Q $\Delta H_{rxn}^{298}(R4) = -144.4$ kJ mol^{-1} is an exact result and combine this with $\Delta H_f^{298}(CH_3CO) = -10.0 \pm 1.2$ kJ mol^{-1} and $\Delta H_f^{298}(O_2) = 0$ kJ mol^{-1} to obtain $\Delta H_f^{298}(CH_3C(O)O_2) = -154.4 \pm 1.2$ kJ mol^{-1}. A more realistic assessment of the uncertainty in this result incorporates ± 5.7 kJ mol^{-1} for the CBS-Q enthalpy (see Table 9) to yield -154.4 ± 5.8 kJ mol^{-1}. One may then substitute the new $CH_3C(O)O_2$ heat of formation into the expression for ΔH_{rxn}^{298}(R1a) to obtain $\Delta H_f^{298}(CH_3C(O)OONO_2) = -240.1 \pm 7.1$ kJ mol^{-1}.

Similar methodology applied to the reactions

$$CH_3CO + O \rightarrow CH_3CO(O)O \qquad \text{(R6)}$$

$$CH_3 + CO_2 \rightarrow CH_3CO(O)O \qquad \text{(R7)}$$

$$CH_3COOH + OH \rightarrow CH_3CO(O)O + H_2O \qquad \text{(R8)}$$

$$CH_3COOH + HO_2 \rightarrow CH_3CO(O)O + HOOH \qquad \text{(R9)}$$

yields $\Delta H_f^{298}(CH_3C(O)O) = -192.5 \pm 5.8$ kJ mol^{-1} which may then be substituted into R1b to obtain $\Delta H_{rxn}^{298}(R1b) = 121.2 \pm 8.4$ kJ mol^{-1} or into R3 to yield $\Delta(\Delta H_{rxn}^{298}) = 2.4 \pm 7.3$ kJ mol^{-1}. It is important to note the internal consistency of the CBS-Q enthalpies for R6−R9 (see Table 10) since there is no single reaction with a well-determined experimental reaction enthalpy that may be used to derive $\Delta H_f^{298}(CH_3C(O)O)$. However, the symmetry breaking observed in the CBS-Q $CH_3C(O)O$ structure (Table 5) suggests that there may be a small systematic error in the CBS-Q energy for $CH_3C(O)O$.

The PAN thermochemistry derived from the hybrid experimental/CBS-Q approach is summarized in Table 11. These ΔH_f^{298} values are then used to recalculate the experimental reaction enthalpies in Table 10 and the differences between the modified experimental ΔH_{rxn}^{298} and the CBS-Q ΔH_{rxn}^{298} are listed as the Δ(adj) column. The change reduces the rms deviation for the entire reaction set from 12.80 to 4.62 kJ mol^{-1}. The modified thermochemistry now yields a description of the PAN/RO_x reaction set that is consistent with the performance expected from the CBS-Q level of theory. Paradoxically, the energy difference between R1a and R1b, 2.4 ± 7.3 kJ mol^{-1}, becomes smaller with the modified thermochemistry and still cannot explain the large number of thermal dissociation experiments that show PAN decomposes exclusively via channel R1a under ambient conditions. One should also note that the discrepancies between the experimental and CBS-Q reaction enthalpies for R1a and R1b slightly increase when the adjusted formation enthalpy values are used. This deviation is directly linked to the difference between the ΔH_f^{298}(PAN) value determined in this study and the CBS-Q ΔH_f^{298}(PAN).

TABLE 11: PAN Thermochemistry[a]

ΔH_f^{298K}

molecule	this study	JPL 97-4	IUPAC	literature
$CH_3C(O)OONO_2$	-240.1 ± 7.2	-259 ± 20.8	-258	-239 ± 8.4[b] -258 ± 22[c] -259 ± 20.8[d]
$CH_3C(O)O_2$	-154.4 ± 5.8	-172 ± 20.8	-172	-172 ± 20[c,d] -162[e]
$CH_3C(O)O$	-192.5 ± 5.8	-207.5	-207.5	-233[e] -216[f]

ΔH_{rxn}^{298K}

reaction	this study	JPL 97-4	IUPAC	literature
PAN → $CH_3C(O)O_2 + NO_2$	118.8 ± 4.0	120.9 ± 29.6	119.2	118.8 ± 4.0[c] 120.6 ± 5.8[d]
PAN → $CH_3C(O)O + NO_3$	121.2 ± 8.4	125.5 ± 23.5	124.2	
$CH_3C(O)O_2 + NO_2 \rightarrow CH_3C(O)O + NO_3$	2.4 ± 7.3	4.6 ± 23.5	5.0	

[a] All values in units of kJ mol^{-1}. [b] Reference 18. [c] Reference 19. [d] Reference 4. [e] Reference 53. [f] Reference 64.

The heats of formation determined in this work suggest that PAN, $CH_3C(O)O_2$, and $CH_3C(O)O$ are all less exothermic than currently recommended. It is interesting to note that Domalski[18] estimated a PAN heat of formation, $\Delta H_f^{298}(PAN) = -238.5 \pm 8.4$ kJ mol^{-1}, in very good agreement with the value of -240.1 ± 7.1 kJ mol^{-1} derived above. It should be further noted that Bridier et al.[19] based their determination of $\Delta H_f^{298}(PAN) = -258 \pm 20$ kJ mol^{-1} on their experimental measurement of ΔH_{rxn}^{298}(R1a) and a MNDO semiempirical calculation that yielded $\Delta H_f^{298}(CH_3C(O)O_2) = -172 \pm 20$ kJ mol^{-1}. Our determination of ΔH_f^{298}(PAN) has employed the same thermochemical cycle, but the accuracy of the CBS-Q $\Delta H_f^{298}(CH_3C(O)O_2)$ has produced a much improved overall thermochemistry. The LCGTO-LSD calculations of Sicilia et al.,[53] $\Delta H_f^{298}(CH_3C(O)O_2) = -163$ kJ mol^{-1}, are consistent with the present results.

The noticeable discrepancy between the CBS-Q derived $\Delta H_f^{298}(CH_3C(O)O) = -192.5 \pm 5.8$ kJ mol^{-1} and the experimental value of -236 ± 8.2 kJ mol^{-1} obtained from photoionization measurements[64] remains somewhat puzzling. We note that the CBS-Q $\Delta H_f^{298}(CH_3C(O)O)$ is consistent with the thermochemistry of $CH_3C(O)O$ formation from CH_3CO, with hydrogen abstraction from CH_3COOH, and with oxygen atom loss from $CH_3C(O)O_2$. We suggest the possibility that Holmes et al. were not probing the $CH_3C(O)O$ radical in these experiments.

4. Implications for Atmospheric Chemistry. The thermochemical analysis of $HOONO_2$ and PAN dissociation pathways presented above has demonstrated that the ROO−NO_2 and RO−ONO_2 bond strengths are significantly different in these two molecules, yet the peroxy nitrate group dominates the decomposition chemistry for both species. The ROO−NO_2 bond in $HOONO_2$ is approximately 20 kJ mol^{-1} weaker than the corresponding bond in PAN, and the $\Delta(\Delta H_{rxn}^{298})$ between the RO + NO_3 and ROO + NO_2 channels in $HOONO_2$ is approximately 65 kJ mol^{-1} while the PAN decompositions appear to be nearly isoenergetic. Despite these differences, all

experimental evidence indicates that the thermal dissociations of $HOONO_2$ and PAN occur solely via the ROO + NO_2 channel. This suggests that there is a substantial barrier to decomposition via RO + NO_3 whether or not that channel is significantly more endothermic. Kirchner et al.[14] have recently reported a systematic procedure for evaluating the thermal stability of peroxy nitrates; it will be interesting to discover whether the thermal decomposition branching ratios observed for $HOONO_2$ and PAN persist for other members of this class. However, thermal dissociation into ROO + NO_2 must be considered as the principal atmospheric fate of peroxy nitrates at low altitudes until a counterexample has been found.

The HOMO and LUMO orbitals for PAN suggest that the lowest energy electronic transition is localized on the NO_2 chromophore, as is typical for RNO_2 molecules.[65−67] The photodissociation process should thus reflect the redistribution of the photoexcitation energy from the NO_2 group throughout the remainder of the molecule. Since the weak ROO−NO_2 and RO−ONO_2 bonds are the first bonds encountered in this process, one expects that the ROO + NO_2 channel should dominate the photofragment yield with a smaller contribution from the RO + NO_3 channel. This prediction agrees with the results of Mazely et al., who observed quantum yields of 0.83 ± 0.09 and 0.3 ± 0.1 for NO_2 and NO_3, respectively, from 248 nm PAN photodissociation.[16,17] The observation of NO_3 places an upper limit on the barrier to RO + NO_3, 480 kJ mol^{-1} relative to PAN or 355 kJ mol^{-1} above the thermodynamic threshold for R1b, although the true barrier height is probably much lower. Photodissociation of $HOONO_2$ at 248 nm results in similar NO_2 and NO_3 quantum yields[68] as well as visible emission from electronically excited NO_2 fragments.[69] One should also expect NO_2* emission from PAN since the 248 nm photodissociations of PAN and $HOONO_2$ both deposit ∼300 kJ mol^{-1} of excess energy in the photofragments.

Recently, anomalies in HO_x concentrations observed in the Arctic at high solar zenith angle have been attributed to $HOONO_2$ photolyzed via OH overtone transitions.[70,71] The energy in a quantum of the OH stretching mode (ν_1) of $HOONO_2$ is approximately 42 kJ mol^{-1}; thus, the thermodynamic information derived above indicates that $HOONO_2$ will have sufficient internal energy to dissociate into HO_2 + NO_2 for excitation into the OH stretching overtones $n\nu_1$ for $n \geq 3$. The thermodynamic threshold for dissociation into OH + NO_3 lies very near the $4\nu_1$ excitation energy so that both dissociation channels should be considered for absorption via $n\nu_1$ overtones with $n \geq 4$. Overtone-induced dissociation of $HOONO_2$ should provide an interesting dynamical contrast to UV photodissociation since all of the energy begins in the OH local mode instead of in the NO_2 group. It is unclear what effect this will have on the product branching ratios for cases in which both dissociation channels are energetically possible.

The CH overtone absorptions in PAN should be of similar strength to the OH overtones in $HOONO_2$. However, overtone photodissociation of PAN seems much less probable given the large number of low-frequency vibrations in the acetyl portion of the molecule. The CH local modes must couple through the acetyl C−C chain before reaching the weak RO−O and ROO−NO_2 bonds unlike $HOONO_2$, where the OH local mode couples directly to the peroxynitrate linkage. The thermodynamic thresholds listed in Table 11 indicate that CH overtones $n \geq 4$ should provide sufficient energy for PAN to dissociate via either R1a or R1b. Thermal dissociation experiments indicate a significant barrier to the $CH_3C(O)O$ + NO_3 dissociation channel, but experiments combining tunable overtone-induced photodissociation with NO_3 product detection might provide a measure of this barrier height.

Acknowledgment. The authors thank S. P. Sander (JPL) for helpful discussions. We acknowledge the Jet Propulsion Laboratory, California Institute of Technology, for allowing us to use their Cray computers to complete this work. The Cray Supercomputers were provided by funding from the NASA Office of Mission to Planet Earth, Aeronautics, and Space Science. C.E.M. acknowledges the Camille and Henry Dreyfus Foundation for a Faculty Start-up Grant. The Gaussian 98W software used at Haverford was purchased in part with funds from the Quaker Chemical Foundation.

References and Notes

(1) Stephens, E. R.; Hanst, P. L.; Doerr, R. C.; Scott, W. E. *Ind. Chem. Eng.* **1956**, *48*, 1498−1504.
(2) Singh, H. B.; Salas, L. J.; Viezee, W. *Nature* **1986**, *321*, 588−91.
(3) Ridley, B. A.; Shetter, J. D.; Gandrud, B. W.; Salas, L. J.; Singh, H. B.; Carroll, M. A.; Hubler, G.; Albritton, D. L.; Hastie, D. R.; Schiff, H. I.; Mackay, G. I.; Karechi, D. R.; Davis, D. D.; Bradshaw, J. D.; Rodgers, M. O.; Sandholm, S. T.; Torres, A. L.; Condon, E. P.; Gregory, G. L.; Beck, S. M. *J. Geophys. Res.* **1990**, *95*, 10179−92.
(4) Zabel, F. *Z. Phys. Chem.* **1995**, *188*, 119−142.
(5) Orlando, J. J.; Tyndall, G. S.; Calvert, J. G. *Atmos. Environ. A* **1992**, *26*, 3111−3118.
(6) Sehested, J.; Christensen, L. K.; Mogelberg, T.; Nielsen, O. J.; Wallington, T. J.; Guschin, A.; Orlando, J. J.; Tyndall, G. S. *J. Phys. Chem. A* **1998**, *102*, 1779−1789.
(7) Niki, H.; Maker, P. D.; Savage, C. M.; Breitenbach, L. P. *Int. J. Chem. Kinet.* **1985**, *17*, 525−534.
(8) Seefeld, S.; Kinnison, D. J.; Kerr, J. A. *J. Phys. Chem. A* **1997**, *101*, 55−59.
(9) Hendry, D. G., et al. *J. Am. Chem. Soc.* **1977**, *99*, 3198−3199.
(10) Talukdar, R. K.; Burkholder, J. B.; Schmoltner, A. M.; Roberts, J. M.; Wilson, R. R.; Ravishankara, A. R. *J. Geophys. Res.* **1995**, *100*, 14163−14173.
(11) DeMore, W. B.; Sander, S. P.; Golden, D. M.; Hampson, R. F.; Kurylo, M. J.; Howard, C. J.; Ravishankara, A. R.; Kolb, C. E.; Molina, M. J. *Chemical Kinetcs and Photochemical Data for Use in Stratospheric Modeling*; Evaluation no. 12; NASA JPL, 1997.
(12) Atkinson, R.; Baulch, D. L.; Cox, R. A.; Hampson, R. F.; Kerr, J. A.; Rossi, M. J.; Troe, J. *J. Phys. Chem. Ref. Data* **1997**, *26*, 1329−1499.
(13) Grosjean, D.; Grosjean, E.; Williams, E. L. *J. Air Waste Manage. Assoc.* **1994**, *44*, 391−396.
(14) Kirchner, F.; Mayer-Figge, A.; Zabel, F.; Becker, K. H. *Int. J. Chem. Kinet.* **1999**, *31*, 127−144.
(15) Roberts, J. M.; Bertman, S. B. *Int. J. Chem. Kinet.* **1992**, *24*, 297−307.
(16) Mazely, T. L.; Friedl, R. R.; Sander, S. P. *J. Phys. Chem.* **1995**, *99*, 8162−8169.
(17) Mazely, T. L.; Friedl, R. R.; Sander, S. P. *J. Phys. Chem. A* **1997**, *101*, 7090−7097.
(18) Domalski, E. S. *Environ. Sci. Technol.* **1971**, *5*, 443−444.
(19) Bridier, I.; Caralp, F.; Loirat, H.; Lesclaux, R.; Veyret, B.; Becker, K. H.; Reimer, A.; Zabel, F. *J. Phys. Chem.* **1991**, *95*, 3594−3600.
(20) Jursic, B. S. *THEOCHEM* **1996**, *370*, 65−69.
(21) Saxon, R. P.; Liu, B. *J. Phys. Chem.* **1985**, *89*, 1227−1232.
(22) Chen, Z.; Hamilton, T. P. *J. Phys. Chem.* **1996**, *100*, 15731−15734.
(23) Petersson, G. A.; Tensfeldt, T. G.; Montgomery, J. A., Jr. *J. Chem. Phys.* **1991**, *94*, 6091−101.
(24) Frisch, M. J.; Trucks, G. W.; Schlegel, H. B.; Scuseria, G. E.; Robb, M. A.; Cheeseman, J. R.; Zakrzewski, V. G.; Montgomery, J. A., Jr.; Stratmann, R. E.; Burant, J. C.; Dapprich, S.; Millam, J. M.; Daniels, A. D.; Kudin, K. N.; Strain, M. C.; Farkas, O.; Tomasi, J.; Barone, V.; Cossi, M.; Cammi, R. *Gaussian 98*, revision A.3; Gaussian, Inc.: Pittsburgh, PA, 1998.
(25) Head Gordon, M.; Pople, J. A.; Frisch, M. J. *Chem. Phys. Lett.* **1988**, *153*, 503−506.
(26) Head Gordon, M.; Head Gordon, T. *Chem. Phys. Lett.* **1994**, *220*, 1−2.
(27) Frisch, M. J.; Head Gordon, M.; Pople, J. A. *Chem. Phys. Lett.* **1990**, *166*, 275−280.
(28) Frisch, M. J.; Head Gordon, M.; Pople, J. A. *Chem. Phys. Lett.* **1990**, *166*, 281−289.
(29) Becke, A. D. *J. Chem. Phys.* **1993**, *98*, 5648−52.
(30) Pople, J. A.; Head Gordon, M.; Raghavachari, K. *J. Chem. Phys.* **1987**, *87*, 5968−5975.

(31) Ditchfield, R.; Hehre, W. J.; Pople, J. A. *J. Chem. Phys.* **1971**, *54*, 724−728.
(32) Hehre, W. J.; Ditchfield, R.; Pople, J. A. *J. Chem. Phys.* **1972**, *56*, 2257−2261.
(33) Hariharan, P. C.; Pople, J. A. *Mol. Phys.* **1974**, *27*, 209−214.
(34) Gordon, M. S. *Chem. Phys. Lett.* **1980**, *76*, 163−168.
(35) Hariharan, P. C.; Pople, J. A. *Theor. Chim. Acta* **1973**, *28*, 213−22.
(36) Clark, T.; Chandrasekhar, J.; Spitznagel, G. W.; von Ragué Schleyer, P. *J. Comput. Chem.* **1983**, *4*, 294−301.
(37) Frisch, M. J.; Pople, J. A.; Binkley, J. S. *J. Chem. Phys.* **1984**, *80*, 3265−3269.
(38) Woon, D. E.; Dunning, T. H., Jr. *J. Chem. Phys.* **1993**, *98*, 1358−1371.
(39) Woon, D. E.; Dunning, T. H., Jr. *J. Chem. Phys.* **1994**, *100*, 2975−2988.
(40) Woon, D. E.; Dunning, T. H., Jr. *J. Chem. Phys.* **1995**, *103*, 4572−4585.
(41) Wilson, A. K.; van Mourik, T.; Dunning, T. H., Jr. *THEOCHEM* **1996**, *388*, 339−349.
(42) Dunning, T. H., Jr. *J. Chem. Phys.* **1989**, *90*, 1007−1023.
(43) Kendall, R. A.; Dunning, T. H., Jr.; Harrison, R. J. *J. Chem. Phys.* **1992**, *96*, 6796−6806.
(44) Ochterski, J. W.; Petersson, G. A.; Montgomery, J. A., Jr. *J. Chem. Phys.* **1996**, *104*, 2598−2619.
(45) Petersson, G. A.; Al Laham, M. A. *J. Chem. Phys.* **1991**, *94*, 6081−6090.
(46) Montgomery, J. A., Jr.; Frisch, M. J.; Ochterski, J. W.; Petersson, G. A. *J. Chem. Phys.* **1999**, *110*, 2822−2827.
(47) Pople, J. A.; Head Gordon, M.; Fox, D. J.; Raghavachari, K.; Curtiss, L. A. *J. Chem. Phys.* **1989**, *90*, 5622−5629.
(48) Curtiss, L. A.; Jones, C.; Trucks, G. W.; Raghavachari, K.; Pople, J. A. *J. Chem. Phys.* **1990**, *93*, 2537−2545.
(49) Curtiss, L. A.; Raghavachari, K.; Trucks, G. W.; Pople, J. A. *J. Chem. Phys.* **1991**, *94*, 7221−7230.
(50) Curtiss, L. A.; Raghavachari, K.; Pople, J. A. *J. Chem. Phys.* **1993**, *98*, 1293−1298.
(51) Curtiss, L. A.; Raghavachari, K.; Pople, J. A. *J. Chem. Phys.* **1995**, *103*, 4192−4200.
(52) Suenram, R. D.; Lovas, F. J.; Pickett, H. M. *J. Mol. Spectrosc.* **1986**, *116*, 406−421.
(53) Sicilia, E.; Dimaio, F. P.; Russo, N. *J. Phys. Chem.* **1993**, *97*, 528−530.
(54) Rauk, A.; Yu, D.; Armstrong, D. A. *J. Am. Chem. Soc.* **1994**, *116*, 8222−8228.
(55) Kieninger, M.; Ventura, O. N.; Suhai, S. *Int. J. Quantum Chem.* **1998**, *70*, 253−267.
(56) Litorja, M.; Ruscic, B. *J. Electron. Spectrosc. Relat. Phenom.* **1998**, *97*, 131−146.
(57) Curtiss, L. A.; Krishnan, R.; Redfern, P. C.; Pople, J. A. *J. Chem. Phys.* **1997**, *106*, 1063−1079.
(58) Curtiss, L. A.; Raghavachari, K.; Redfern, P. C.; Pople, J. A. *Chem. Phys. Lett.* **1997**, *270*, 5−6.
(59) Curtiss, L. A.; Raghavachari, K.; Redfern, P. C.; Stefanov, B. B. *J. Chem. Phys.* **1998**, *108*, 692−697.
(60) Montgomery, J. A., Jr.; Frisch, M. J.; Ochterski, J. W.; Petersson, G. A.; Raghavachari, K.; Zakrzewski, V. G. *J. Chem. Phys.* **1998**, *109*, 6505−6506.
(61) Petersson, G. A.; Malick, D. K.; Wilson, W. G.; Ochterski, J. W.; Montgomery, J. A., Jr.; Frisch, M. J. *J. Chem. Phys.* **1998**, *109*, 10570−10579.
(62) Niiranen, J. T.; Gutman, D.; Krasnoperov, L. N. *J. Phys. Chem.* **1992**, *96*, 5881−5886.
(63) Bauschlicher, C. W. *J. Phys. Chem.* **1994**, *98*, 2564−2566.
(64) Holmes, J. L.; Lossing, F. P.; Mayer, P. M. *J. Am. Chem. Soc.* **1991**, *113*, 9723−9728.
(65) Johnston, H. S.; Miller, C. E.; Oh, B. Y.; Patten, K. O.; Sisk, W. N. *J. Phys. Chem.* **1993**, *97*, 9890−9903.
(66) Miller, C. E.; Johnston, H. S. *J. Phys. Chem.* **1993**, *97*, 9924−9933.
(67) Sisk, W. N.; Miller, C. E.; Johnston, H. S. *J. Phys. Chem.* **1993**, *97*, 9916−9923.
(68) Sander, S. Personal communication.
(69) MacLeod, H.; Smith, G. P.; Golden, D. M. *J. Geophys. Res.* **1988**, *93*, 3813−3823.
(70) Donaldson, D. J.; Frost, G. J.; Rosenlof, K. H.; Tuck, A. F.; Vaida, V. *Geophys. Rev. Lett.* **1997**, *24*, 2651−2654.
(71) Wennberg, P. O.; Salawitch, R. J.; Donaldson, D. J.; Hanisco, T. F.; Lanzendorf, E. J.; Perkins, K. K.; Lloyd, S. A.; Vaida, V.; Gao, R. S.; Hintsa, E. J.; Cohen, R. C.; Swartz, W. H.; Kusterer, T. L.; Anderson, D. E. *Geophys. Rev. Lett.* **1999**, *26*, 1373−1376.